



On the success rate of the farside seismic imaging of active regions

I. González Hernández,¹ F. Hill,¹ P. H. Scherrer,² C. Lindsey,³ and D. C. Braun³

Received 13 November 2009; revised 3 March 2010; accepted 18 March 2010; published 10 June 2010.

[1] Seismic maps of the nonvisible side of the Sun (farside) have been used for almost a decade to follow large active regions before they rotate to face the Earth. Preliminary efforts to quantify the success rate of the technique (seismic holography) have been published with Michelson Doppler Imager (MDI) data. In this paper we present a thorough statistical analysis of 3 complete years of farside seismic maps (2003–2005) calculated using both Global Oscillation Network Group (GONG) data and a combined set of GONG and MDI data. A comparison with NOAA data of the frontside of the Sun during the same period shows that seismic maps detect about 40% of the total active regions that appear at the east limb of the Sun with a confidence level higher than 60%. The relationship found during this work between the seismic signature and the confidence level allows us to automatically highlight candidates in the farside seismic maps and to assign them the corresponding probability of appearance on the frontside.

Citation: González Hernández, I., F. Hill, P. H. Scherrer, C. Lindsey, and D. C. Braun (2010), On the success rate of the farside seismic imaging of active regions, *Space Weather*, 8, S06002, doi:10.1029/2009SW000560.

1. Introduction

[2] For almost a decade now, helioseismic holography, a technique developed by *Lindsey and Braun* [1990, 1997], has been used to map magnetic regions on the nonvisible disk of the Sun. When waves interact with active regions, they experience a phase shift, leaving a seismic signature that can be measured by observing the wave field at a different location on the solar surface. In particular, this seismic signature of active regions can be measured by observing waves that have traveled all the way from the farside to the frontside of the Sun. Since its first application in 2000 to Michelson Doppler Imager (MDI) [*Scherrer et al.*, 1995] data [*Lindsey and Braun*, 2000a], the method has proven its capability to locate large active regions on the farside solar surface. It also provides the capability to monitor the migration of active regions around the farside for many days before facing the Earth and possibly impacting space weather.

[3] In 2003 a preliminary version of farside images calculated from the Global Oscillation Network Group (GONG) [*Harvey et al.*, 1996] went online. Since 2005 continuous full-hemisphere farside maps have been calculated from this ground-based instrument. The farside maps are calculated twice daily and can be accessed at [http://gong.](http://gong.nso.edu/data/farside/for GONG observations and http://soi.stanford.edu/data/farside/for MDI observations)

[nso.edu/data/farside/for GONG observations and http://soi.stanford.edu/data/farside/for MDI observations.](http://soi.stanford.edu/data/farside/for MDI observations)

[4] Efforts to improve the farside maps calculated from helioseismology have continued: *González Hernández et al.* [2007] found a relationship between the farside seismic signatures of active regions and the corresponding magnetic field strengths. The correlation between farside phase signature and magnetic field strength is consistent with an approximately logarithmic relationship between the two above a critical field of ~ 10 G. This empirical calibration is currently used to calibrate the farside maps. *Zhao* [2007] demonstrated that another local helioseismology technique, time-distance, can also be used to obtain seismic maps of active regions on the farside of the Sun. *González Hernández et al.* [2009] found a diffuse signature in the farside maps that changes with the solar cycle. This is now being subtracted from the maps to accentuate the more compact active regions. *Zhao* [2007] and *Ilonidis et al.* [2009] show that adding more waves that follow different raypaths to the analysis improves the signal-to-noise ratio in the farside maps. As new research is completed, the calculated maps become more precise and useful for applications such as space weather and irradiance forecasting models (see work by *Fontenla et al.* [2009] for the latter).

[5] The first attempt to quantify the reliability of the method was made by *Buder and Scherrer* [2006]. Here we present a deeper investigation of the reliability of mapping active regions at the nonvisible disk of the Sun using helioseismic holography. We compare the location of

¹National Solar Observatory, Tucson, Arizona, USA.

²HEPL, Stanford University, Stanford, California, USA.

³CoRA Division, NorthWest Research Associates, Boulder, Colorado, USA.

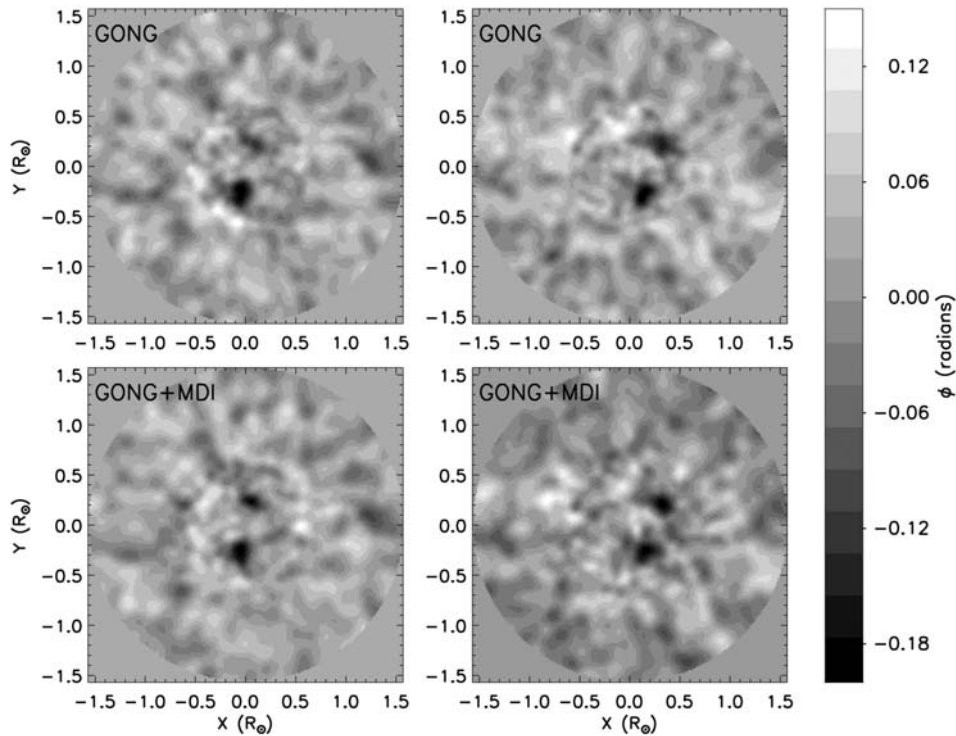


Figure 1. Postel projections of the farside maps of ϕ for (left) 12 November and (right) 13 November 2003 for (top) GONG and (bottom) the average of GONG and MDI showing the strong seismic signatures close to the center (antipode of the Earth-facing hemisphere) of active regions NOAA 10488(10507) and NOAA 10486(10508).

farside candidates calculated with the GONG instrument, and with a combined set of GONG and MDI, with the National Oceanic and Atmospheric Administration (NOAA) database of active regions subsequently appearing on the nearside of the Sun to determine a confidence level as a function of the measured phase shift. This confidence level is defined as the percent of farside candidates that are ultimately validated by the appearance of a numbered NOAA active region emerging from the limb. We also estimate the success rate, that is, the fraction of the total possible number of active regions that are actually detected on the farside.

2. Data Analysis

[6] The farside seismic maps used for this work were calculated using the phase-sensitive seismic holography technique described by *Lindsey and Braun* [2000b] and *Braun and Lindsey* [2001]. The technique is based on the principle that there is a phase shift (traveltime delay) between waves going into and out of an active region [*Braun et al.*, 1992].

[7] Each map is calculated using 1 day series of data with a cadence of 1 min. The calculated maps represent the phase shift between waves going into and out of a particular location (focus) on the Sun's far surface. In the

analysis, the propagation of the waves in the quiet photosphere is represented by a model [see *Lindsey and Braun*, 2000b]. When the focus is located in the quiet photosphere, the phase shift with respect to the model is close to zero; if the focus is located in an area of strong magnetic field, the phase is shifted backward relative to the model. Waves following a raypath that bounces zero, one, or two times in the solar surface before arriving at the observational pupil on the frontside are included in the analysis to complete the full-hemisphere farside maps [*Braun and Lindsey*, 2001].

[8] Figure 1 shows Postel projections of farside phase shifts for 12 and 13 November 2003 for GONG and the average between GONG and MDI. Dark areas in the maps correspond to relatively negative phase signatures, ϕ , manifested by active regions. In these particular maps, active regions NOAA 10486(10508) and NOAA 10488 (10507) are seen on the farside approximately 7–8 days after they rotated across the west limb of the Sun, disappearing from direct view. They appeared on the nearside in the succeeding Carrington rotation. The Postel projections are reprojected onto a longitude-sin(latitude) grid (see Figure 2).

[9] The period selected for the analysis spans January 2003 to December 2005. This appears to be an optimal time interval, during the declining phase of cycle 23, for this

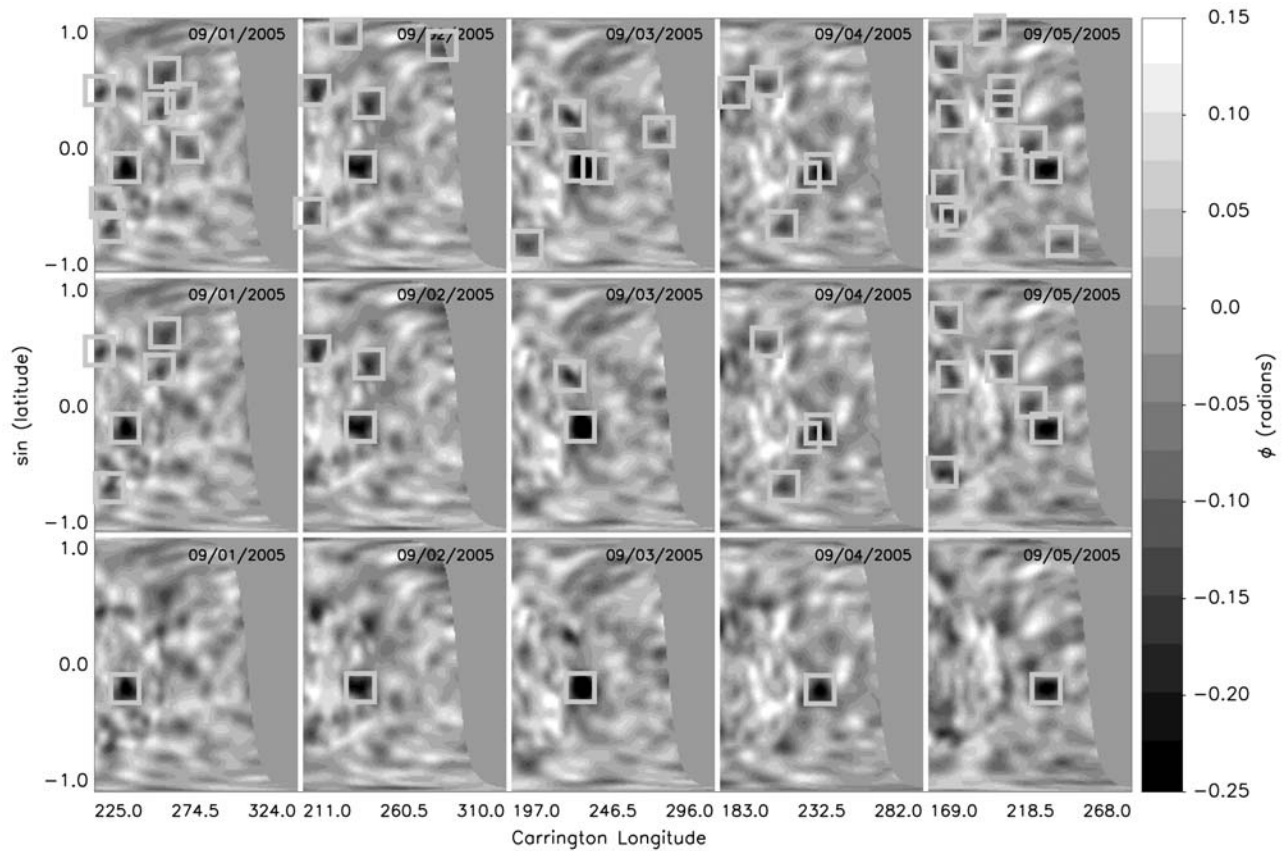


Figure 2. Active region candidates in farside maps calculated for the period 1–5 September 2005. Candidates are selected using different threshold levels for ϕ : (top) -0.11 , (middle) -0.14 , and (bottom) -0.20 rad. The bottom set clearly identifies active region NOAA 10808, which appears at the east limb on 7 September 2005.

study. First, we have simultaneous data from GONG and MDI instruments, albeit with different resolution. Second, the Sun presents enough activity to provide a significant set of active regions, yet the spatial and temporal cadences of the surface activity allow us to isolate and clearly identify the active regions. A more active phase of the cycle would be less discriminating of false positive farside signatures because of a high probability of an active region appearing in a particular location anyway, and a less active period would render an insufficient sample.

[10] We only include a farside map in our analysis if the duty cycle of the data used to calculate the map is greater than 85%. With this constraint, our samples consist of 797 daily GONG farside maps and a total combined GONG and MDI set of 1069 maps. For the combined set, we use an average when GONG and MDI maps are available or either GONG or MDI maps if only one of them is present.

[11] We developed an algorithm to identify candidates from farside signatures as indicative of actual active regions. A precandidate is defined as a local phase shift minimum above a particular signal threshold in a single map. The status of candidate is only assigned to pre-

candidates that remain above the threshold in the synoptic maps for at least 2 consecutive days. Persistence is imposed to identify weaker active regions since the phase shift associated with them is close to the noise level. However, while the noise is short lived, the phase shift due to the existence of active regions remains present from map to map. Varying the phase shift threshold, we obtain different numbers of precandidates for the same map. GONG farside maps showing the detected precandidates with a negative phase shift larger than -0.11 , -0.14 , and -0.20 rad are shown in Figure 2, projected onto a longitude-sin(latitude) grid. Only longitudes within 90° of the east limb are included in the analysis, that is, only active regions that are expected to rotate onto the frontside in 7 days or less.

[12] Once the candidates are identified in the farside maps for the different phase shift threshold levels, the locations are matched with those of the NOAA active regions subsequently appearing on the frontside to validate the detections. Since NOAA assigns numbers to active regions that are already at no more than 60°E – 70°E heliocentric longitude, our automatic identification pro-

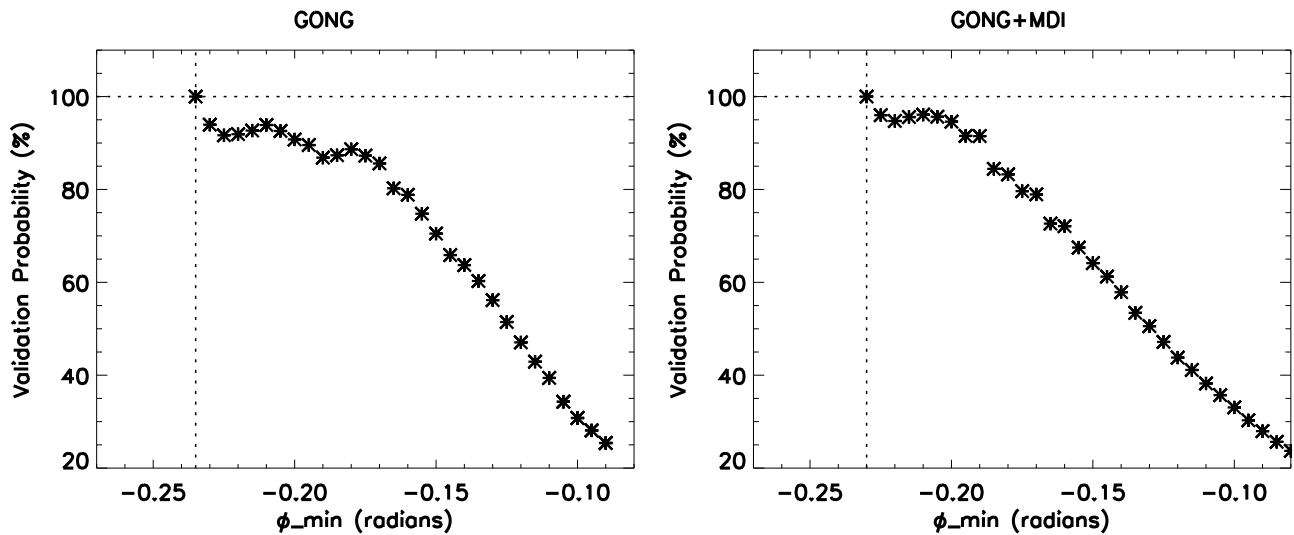


Figure 3. Positive detections versus seismic signatures, ϕ , for active regions detected in (left) GONG and (right) the GONG and MDI combined set farside maps. Stronger signals lead to more accurate predictions.

cess has to account for this. This introduces a potential error due to active regions that may emerge between the time of our observations in the east limb and the time when NOAA identifies them. To eliminate this possibility, a visual inspection of the matched active regions has been conducted, and those emerging on the frontside have been removed from the identified set. The same analysis is done for the farside images calculated from GONG data and from the combined GONG-MDI set.

3. Validation and Success Rate

[13] Figure 3 shows positive identifications, as a validation probability, for GONG phase maps and the combined set of GONG and MDI. The validation probability is plotted against the phase shift threshold used to identify the candidates. In Figure 3, ϕ represents the maximum negative phase shift, and the validation probability represents the minimum probability achieved for a particular value of ϕ . It can be seen that, in general, the validation probability is greater for larger thresholds, which are found to correspond to larger, stronger active regions [González Hernández et al., 2007]. The sample of candidates significantly decreases above the phase shift threshold of 0.15 rad; hence, the results became noisier at large thresholds. Any candidate with an associated negative phase shift larger than 0.235 for GONG or with a negative signature stronger than 0.23 for the combination of GONG and MDI is guaranteed to appear at the frontside. Active regions detected by GONG with a negative phase shift larger than 0.235 for at least 2 days on the farside are presented in Table 1. The maximum area and Hale complexity classification of these active regions, once on the frontside, are included in the tabulation. Despite the expected evolution of the magnetic configuration, most of these active regions that show large

farside signatures remain large and complex as they rotate into view on the nearside.

[14] To evaluate the completeness of the identified set and to calculate the success rate, we estimate the total number of active regions that appeared on the east solar limb during the 3 year interval considered. Visual inspection of a sample of magnetograms and the NOAA archives shows that active regions appearing at the east limb are only recorded and named by NOAA when they are close to the heliocentric longitude of 60°E. We developed an algorithm that extracted all of the active regions with a recorded heliocentric longitude larger than 55°E for the studied period and consider this group to be the total number of active regions coming from the farside. Once the set was automatically identified, we visually inspected

Table 1. Active Regions That Were Detected in the GONG Farside Seismic Maps With a Signal Corresponding to a 100% Confidence Level for at Least 1 Day

NOAA Active Region	East Limb Date	Maximum $\langle\phi\rangle$	Area ^a	Hale Complexity Classification
10380	6 Jun 2003	-0.292	680	$\beta\gamma$
10397	27 Jun 2003	-0.291	930	$\beta\gamma\delta$
10409	12 Jul 2003	-0.285	490	$\beta\gamma$
10486	22 Oct 2003	-0.342	2610	β
10506	18 Nov 2003	-0.280	120	$\beta\gamma$
10508	19 Nov 2003	-0.314	700	$\beta\gamma$
10536	1 Jan 2004	-0.280	980	$\beta\gamma\delta$
10652	16 Jul 2004	-0.260	2010	$\beta\gamma\delta$
10663	19 Aug 2004	-0.262	230	$\beta\gamma$
10667	1 Sep 2004	-0.240	340	β
10732	5 Feb 2005	-0.313	90	$\beta\gamma$
10756	24 Apr 2005	-0.259	1030	$\beta\delta$
10792	28 Jul 2005	-0.265	440	$\beta\gamma\delta$
10808	7 Sep 2005	-0.292	1430	$\beta\gamma\delta$

^aArea is in 10^{-6} solar hemispheres.

Table 2. Active Regions Detected by the Farside Seismic Maps Calculated With Both Instruments Compared to NOAA Number of Active Regions Appearing From the East Limb

Confidence Level	NOAA	GONG	GONG and MDI
Any	254	188	219
≥60%	254	94	99

the corresponding magnetograms for a few days previous to the NOAA identification (closer to the east limb) to confirm that those active regions did not emerge on the frontside but rotated from the farside. Under these specifications, the total number of active regions for 2003–2005 coming from the farside and recorded by NOAA is 254. We detected a total of 188 of these active regions with GONG phase maps and a total of 219 with the combined GONG and MDI data set. Of those, 94 (~37%) were detected for GONG and 99 (~37%) were detected for the combined GONG and MDI phase maps with a confidence level of 60% or more (see Table 2). The possibility of an active region disappearing between the date of detection in the farside maps and the date of appearance on the frontside leaves some uncertainty in our determination of false positives. However, the farside active regions detected by seismic inferences are generally large and/or strong ones [González Hernández *et al.*, 2007], for which the decay time is expected to be long [Hathaway and Choudhary, 2008]. Hence, we expect the probability of an active region detected on the farside disintegrating within 7 days to be small.

[15] The increase in the detection rate achieved by combining both instruments could have several explanations. First, the detection algorithm developed relies on finding a strong signal in the same place for 2 consecutive days. The combined set of farside maps increases the total duty cycle, making the detection method more stable. Second, we find that GONG and MDI maps used for this analysis present different noise distributions as well as different seismic signatures for the same active region. Figure 4 is a scatterplot of the seismic signatures, ϕ , for detected active regions for both GONG (horizontal axis) and MDI (vertical axis) instruments. Each point represents the temporal average of the maximum negative phase shift associated with a particular active region. MDI signatures are systematically larger than GONG signatures for the same active region. Superimposed on the scatterplot is the straight line that best fits the points plotted by least squares. We express this line by

$$\phi_{\text{MDI}} = \phi_0 + A\phi_{\text{GONG}}, \quad (1)$$

where $\phi_0 = -0.13$ rad and $A = 0.53$. We also find that the GONG and MDI noise distributions are different. The different noise could be accounted for by the lower resolution of the MDI images as well as the different implementation of the seismic holography method to account for the two different data sets (e.g., the merging of the

central and peripheral parts of the farside map is dependent on mode sensitivity), but more research is necessary to properly understand the differences.

4. Discussion and Future Work

[16] We have shown that the seismic holography technique is able to detect 37% of the total active regions that appear at the east limb of the Sun with a confidence level of at least 60% for farside maps calculated with GONG data and that the detection rate can be improved by combining farside maps calculated with both GONG and MDI instruments. We have found a relationship between the strength of the signal of an active region in the farside maps and the confidence level of that active region persisting to face the Earth.

[17] The results presented in this paper are now used routinely in the GONG farside map calculations. Figure 5 shows a comparison between the new 2 day average calibrated images (grey) and the original daily farside maps (yellow). The sequence spans from 14 to 17 September 2009 and shows the first active region of the new cycle detected by the seismic farside maps. The active region (NOAA 11026) later appeared at the frontside of the Sun on 20 September 2009. The statistical results have been used to automatically highlight the active region (in red) and to assign a confidence level. Only candidates with a seismic signature associated with a confidence level of 70% or higher are circled. In Figure 5, the map corresponding to 15 September 2009 shows a weaker signature for the farside candidate, below the 70% confidence level.

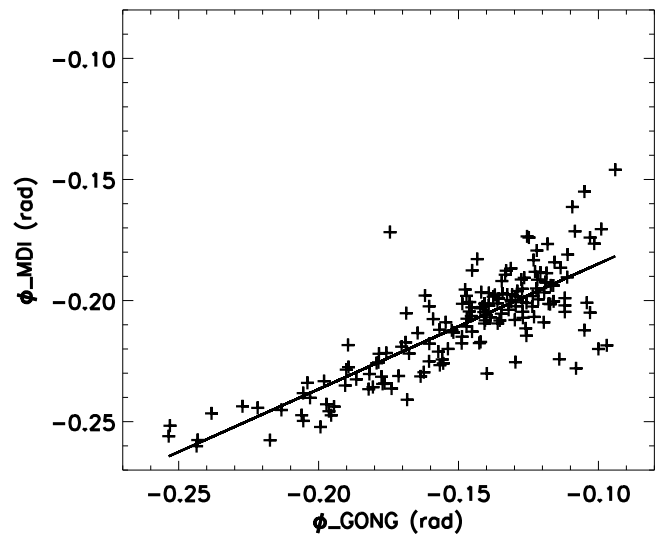


Figure 4. Scatterplot of the seismic signatures of active regions calculated with GONG and MDI data. Each point represents a temporal average of the signatures of a particular active region detected with one instrument versus the other. The signatures are averaged over the different days when the active regions were present in the individual farside maps.

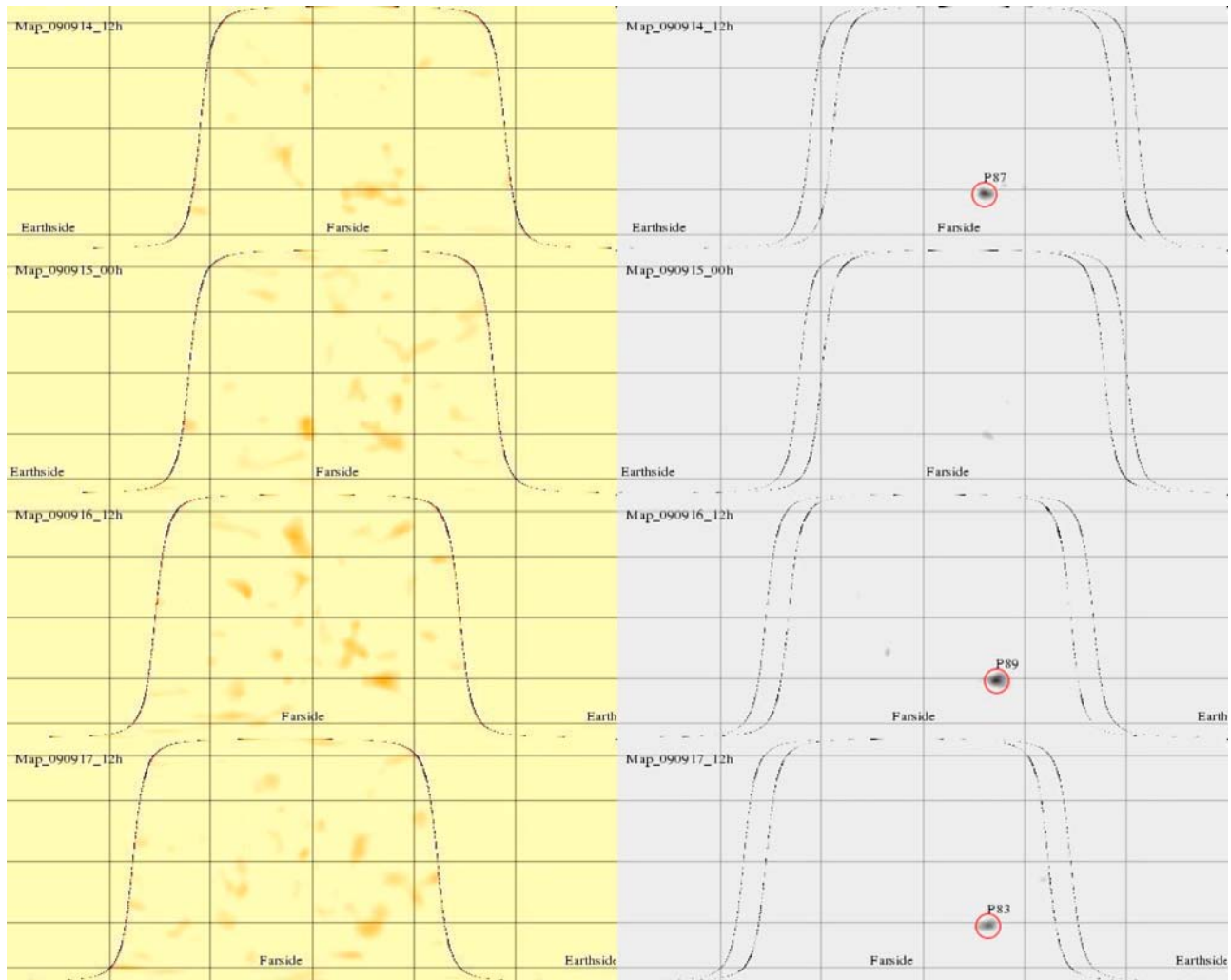


Figure 5. Comparison between (left) traditional daily farside maps and (right) the new averaged (calibrated) ones. In the new maps the noise is reduced substantially and the candidates are highlighted automatically in red. This series of maps was calculated from 14 to 17 September 2009 and shows the first active region of the new cycle detected by the seismic farside maps. The active region later appeared at the frontside of the Sun on 20 September 2009 (NOAA 11026).

[18] The use of farside maps for space weather forecasting is increasing. The forecast center at NOAA's Space Weather Prediction Center in Boulder and the Australian Ionospheric Prediction Service now routinely use helioseismic farside maps. Farside seismic maps have been shown to improve the short-term forecast of the UV solar irradiance [Fontenla *et al.*, 2009] and will be incorporated into the satellite drag predictions provided by Space Environment Technologies (K. Tobiska, private communication, 2009).

[19] Several research lines are open to further improve the signal-to-noise ratio in the seismic farside maps. The existence of two methods for computing the maps, seismic holography and time-distance helioseismology, will contribute to a better understanding of the noise from solar,

instrumental, and data analysis sources. Time-distance analysis of artificial data has shown that the accuracy of acoustic traveltime farside maps depends on the size and location of active regions [Hartlep *et al.*, 2008]. We are at the early stages of analyzing the same artificial set of data with seismic holography. Work is under way to improve the model (Green's functions) used by seismic holography [Pérez Hernández and González Hernández, 2010]. A better model will lead to a better signal-to-noise ratio in the farside maps and will ultimately lead to an improved tool for space weather forecasters.

[20] The GONG network is expected to upgrade the near-real-time data currently used to calculate the daily farside maps to high resolution in the near future. The upcoming launch of the Solar Dynamics Observatory

(SDO) satellite with Helioseismic and Magnetic Imager (HMI) on board will provide a new higher-resolution continuous set of data. After the end of MDI operation, the combination of GONG and HMI data should provide continuing observations for space weather forecasts.

[21] **Acknowledgments.** This work utilized data obtained by the Global Oscillation Network Group (GONG) program, managed by the National Solar Observatory, which is operated by AURA, Inc., under a cooperative agreement with the National Science Foundation. The data were acquired by instruments operated by the Big Bear Solar Observatory, High Altitude Observatory, Learmonth Solar Observatory, Udaipur Solar Observatory, Instituto de Astrofísica de Canarias, and Cerro Tololo Interamerican Observatory. SOHO is a project of international cooperation between ESA and NASA. This work has been supported by the NASA Living With a Star Targeted Research and Technology program and the Stellar Astrophysics branch of the National Science Foundation.

References

- Braun, D. C., and C. Lindsey (2001), Seismic imaging of the far hemisphere of the Sun, *Astrophys. J.*, 560, L189–L192.
- Braun, D. C., T. L. Duvall Jr., B. J. Labonte, S. M. Jefferies, J. W. Harvey, and M. A. Pomerantz (1992), Scattering of p-modes by a sunspot, *Astrophys. J.*, 391, L113–L116.
- Buder, I., and P. H. Scherrer (2006), Quantitative study of solar farside observations to predict active regions, *Eos Trans. AGU*, 87(52), Fall Meet. Suppl., Abstract SH33B-0412.
- Fontenla, J. M., E. Quémérais, I. González Hernández, C. Lindsey, and M. Haberreiter (2009), Solar irradiance forecast and far-side imaging, *Adv. Space Res.*, 44, 457–464.
- González Hernández, I., F. Hill, and C. Lindsey (2007), Calibration of seismic signatures of active regions on the far side of the Sun, *Astrophys. J.*, 669, 1382–1389.
- González Hernández, I., P. Scherrer, and F. Hill (2009), A new way to infer variations of the seismic solar radius, *Astrophys. J.*, 691, L87–L90.
- Hartlep, T., J. Zhao, N. N. Mansour, and A. G. Kosovichev (2008), Validating time-distance far-side imaging of solar active regions through numerical simulations, *Astrophys. J.*, 689, 1373–1378.
- Harvey, J. W., et al. (1996), The Global Oscillation Network Group (GONG) project, *Science*, 272, 1284–1286.
- Hathaway, D. H., and D. P. Choudhary (2008), Sunspot group decay, *Sol. Phys.*, 250, 269–278.
- Ilonidis, S., J. Zhao, and T. Hartlep (2009), Time-distance solar far-side imaging using three-skip acoustic signals, *Sol. Phys.*, 258, 181–189.
- Lindsey, C., and D. C. Braun (1990), Helioseismic imaging of sunspots at their antipodes, *Sol. Phys.*, 126, 101–115.
- Lindsey, C., and D. C. Braun (1997), Helioseismic holography, *Astrophys. J.*, 485, 895–903.
- Lindsey, C., and D. C. Braun (2000a), Seismic images of the far side of the Sun, *Science*, 287, 1799–1801.
- Lindsey, C., and D. C. Braun (2000b), Basic principles of solar acoustic holography, *Sol. Phys.*, 192, 261–284.
- Pérez Hernández, F., and I. González Hernández (2010), Green's functions for far-side seismic images: A polar-expansion approach, *Astrophys. J.*, 711, 853–860.
- Scherrer, P. H., et al. (1995), The Solar Oscillations Investigation—Michelson Doppler Imager, *Sol. Phys.*, 162, 129–188.
- Zhao, J. (2007), Time-distance imaging of solar far-side active regions, *Astrophys. J.*, 664, L139–L142.

D. C. Braun and C. Lindsey, CoRA Division, NorthWest Research Associates, 3380 Mitchell La., Boulder, CO 80301, USA.

I. González Hernández and F. Hill, National Solar Observatory, 950 N. Cherry Ave., Tucson, AZ 85719, USA. (irenegh@nso.edu)

P. H. Scherrer, HEPL, Stanford University, 452 Lomita Mall, Stanford, CA 94305-4085, USA.